Physics – Uspekhi **63** (8) 775 – 781 (2020)

METHODOLOGICAL NOTES PACS numbers: **63.50.–x, 78.30.–j**

Optical phonons with a negative oscillator strength

E A Vinogradov

DOI: https://doi.org/10.3367/UFNe.2020.01.038719

Contents

Abstract. **We discuss the nature of additional (redundant from the point of view of selection rules) optical phonons observed in most crystals with ion–covalent bonds between atoms, including in their solid solutions. These 'redundant' phonons are located in the frequency range of the longitudinal–transverse splitting of fundamental phonons, where the real part of the crystal permittivity is negative. They are also split by the crystal field into transverse and longitudinal phonons such that the frequencies of redundant longitudinal phonons are lower than those of redundant transverse phonons and the oscillator strength of these phonons is negative.**

Keywords: optical phonons, local vibrations, solid solution, oscillator strength, inverted oscillator, effective ion charge, infrared spectroscopy

1. Introduction

The dynamics of the crystal lattice of binary crystals with ion–covalent bonds between A^2B^6 atoms are described well by the simplest model of rigid ions [1, 2]. For a diatomic isotropic crystal with ZnS-type cubic symmetry, the frequencies of transverse, ω_{TO}, and longitudinal, ω_{LO}, phonons are given by [1–3]

$$\omega_{\mathrm{TO}}^2 = \omega_0^2 - \frac{4\pi}{3}\,\frac{e_{\mathrm{B}}^2}{\sigma\mu}\,, \tag{1}$$

$$\omega_{\mathrm{LO}}^2 = \omega_0^2 + \frac{8\pi}{3}\,\frac{e_{\mathrm{B}}^2}{\sigma\mu}\,, \tag{2}$$

where $\omega_0^2 = -(1/\mu)\sum_l \Phi^N\binom{l}{+\,-}$, ω_0 is the frequency of triple-degenerate atomic vibrations with long-range Coulomb forces ignored, $\Phi^N\binom{l}{+\,-}$ are short-range force constants independent of the position of ions with respect to the crystal surface, $\mu = m_1 m_2/(m_1 + m_2)$ is the reduced dipole mass, m_1 and m_2 are the respective masses of positive and negative ions, l is the cell number, and σ is the unite cell volume. The long-range Coulomb field of ions in single crystals partially lifts the degeneracy from triple-degenerate vibrations with the frequency ω_0, splitting it into the double-degenerate transverse vibrations ω_{TO} and nondegenerate longitudinal vibrations ω_{LO}, but not changing the symmetry of atomic vibrations.

As follows from (1) and (2), the frequencies of longitudinal optical phonons must always be higher than the frequencies of transverse phonons:

$$\omega_{\mathrm{LO}}^2 - \omega_{\mathrm{TO}}^2 = \frac{4\pi\, e_{\mathrm{B}}^2}{\sigma\mu}\,, \quad e_{\mathrm{B}} = \frac{\varepsilon_\infty + 2}{3}\, e_{\mathrm{S}}^*\,, \tag{3}$$

where ε_∞ is the crystal permittivity at frequencies greatly exceeding phonon frequencies, and e_{S}^* is the Czigeti charge [4] — the positive and negative macroscopic ion charge used to describe the crystal lattice dynamics in the rigid lattice model [1–3]. We note that when the frequencies of optical phonons are measured, expression (3) gives the Czigeti charge determining the degree of ionicity of an ion–covalent crystal.

Optical phonon frequencies are typically obtained from a standard expression for the complex permittivity $\varepsilon(\omega)$ of a crystal with two atoms in the unit cell in the quasiharmonic approximation [2, 3]:

$$\varepsilon(\omega) = \varepsilon_\infty + \frac{(\varepsilon_0 - \varepsilon_\infty)\omega_{\mathrm{TO}}^2}{\omega_{\mathrm{TO}}^2 - \omega^2 - \mathrm{i}\omega\gamma}\,. \tag{4}$$

The frequencies ω_{TO} of transverse optical phonons (the TO mode) correspond to the maximum of the function $\omega\,\mathrm{Im}\,\varepsilon(\omega)$, while the function $\omega\,\mathrm{Im}\,(-\varepsilon^{-1}(\omega))$ has a maximum at the frequency ω_{LO} of longitudinal optical phonons (the LO mode):

$$\begin{aligned} \omega\,\mathrm{Im}\,\varepsilon(\omega) &= \frac{(\varepsilon_0 - \varepsilon_\infty)\omega_{\mathrm{TO}}^2\gamma}{(\omega - \omega_{\mathrm{TO}})^2 + \gamma^2}\,, \\ \omega\,\mathrm{Im}\,\big(-\varepsilon^{-1}(\omega)\big) &= \frac{(\varepsilon_\infty^{-1} - \varepsilon_0^{-1})\omega_{\mathrm{LO}}^2\gamma}{(\omega_{\mathrm{LO}} - \omega)^2 + \gamma^2}\,. \end{aligned} \tag{5}$$

E A Vinogradov
Institute of Spectroscopy, Russian Academy of Sciences,
ul. Fizicheskaya 5, 108840 Troitsk, Moscow, Russian Federation
E-mail: evinogr@isan.troitsk.ru

Received 27 November 2019, revised 30 December 2019
Uspekhi Fizicheskikh Nauk **190** (8) 829 – 835 (2020)
Translated by M Sapozhnikov; edited by A M Semikhatov

The half-width of the function $\omega\,\mathrm{Im}\,\varepsilon(\omega)$ gives the constant γ determining the decay of phonons. The crystal permittivity $\varepsilon(\omega)$ is usually obtained from an experimental reflection spectrum after the Kramers–Kronig integral transformation. The oscillator strength of TO phonons $S_{\mathrm{TO}} = \varepsilon_0 - \varepsilon_\infty$ can be determined by several methods:

$$\varepsilon_0 = \left(\frac{\sqrt{R_0}+1}{\sqrt{R_0}-1}\right)^2, \quad \varepsilon_\infty = \left(\frac{\sqrt{R_\infty}+1}{\sqrt{R_\infty}-1}\right)^2,$$

where R_0 and R_∞ are reflection coefficients at respective frequencies $\omega \ll \omega_{\mathrm{TO}}$ and $\omega \gg \omega_{\mathrm{LO}}$, which cannot always be measured with high photometric accuracy. The value of $S_{\mathrm{TO}} = \varepsilon_0 - \varepsilon_\infty$ can be determined more accurately from the imaginary part $\mathrm{Im}\,\varepsilon(\omega) = \varepsilon_2(\omega)$ of the permittivity for $\omega = \omega_{\mathrm{TO}}$:

$$\varepsilon_0 - \varepsilon_\infty = \frac{\gamma_{\mathrm{TO}}}{\omega_{\mathrm{TO}}}\,\varepsilon_2(\omega_{\mathrm{TO}})\,, \tag{6}$$

or from the Kramers–Kronig relation

$$\varepsilon_0 - \varepsilon_\infty = \frac{2}{\pi}\int \frac{\varepsilon_2(\omega)}{\omega}\,\mathrm{d}\omega\,. \tag{7}$$

This clear and orderly picture for ideal crystals without crystal lattice defects is distorted by the existence of features in the IR reflection spectra of real crystals with ion and ion–covalent bonds between atoms. The A^2B^6 semiconductor crystals always contain impurity atoms of the same groups of the Periodic system, which are often considered isotopic impurities, and also atomic vacancies. This gives rise to additional local slot or resonance (quasiresonance) vibrational excitations and to the defect-induced density of phonon states [5]. At high concentrations of impurity atoms, solid crystalline solutions can be formed. The compositional disorder of a solid solution modifies structural, vibrational, and optical properties of crystals. These changes lead to the appearance of features in the lattice dynamics of triple substitution solutions: the one- and two-mode or intermediate behavior of vibrational frequencies ω_{TO} and ω_{LO} in the system [6–8]. In most of these crystals, and especially in their triple $A_{1-x}B_xC$ solid solutions, where atoms A and B belong to the same group of the Periodic table, additional (to the selection rules) optical phonons are observed at the center of the Brillouin zone. These redundant optical phonons have inverted longitudinal, $\omega_{\mathrm{LO}}^{\mathrm{add}}$, and transverse, $\omega_{\mathrm{TO}}^{\mathrm{add}}$, frequencies. The most interesting cases are those where $\omega_{\mathrm{LO}}^{\mathrm{add}} < \omega_{\mathrm{TO}}^{\mathrm{add}}$. In solid solutions of polar compounds of the $A_{1-x}B_xC$ type, in contrast to the limit components AC and BC, the elementary cell contains not only the A–C and B–C dipoles but also the A–B dipole, which is an order of magnitude weaker than the main ones [7–10].

In what follows, we consider the appearance of these additional dipoles and related optical phonons and also attempt to explain their nature using the example of single crystals of $Zn_{1-x}Cd_xS$, $Zn_{1-x}Cd_xSe$, $Zn_{1-x}Cd_xTe$, and $ZnSe_xS_{1-x}$ solid solutions.

2. Experiment

The main parameters of the crystal lattice dynamics (optical phonon frequencies ω_{TO} and ω_{LO} in the center of the Brillouin zone ($k \approx 0$), the phonon lifetime, oscillator strengths, etc.) are obtained from experimental IR reflection spectra and Raman spectra. The reflection spectrum gives the permittivity of the crystal containing most of the required parameters:

$$\varepsilon(\omega) = \varepsilon_\infty + \sum_{j=1}^{n} \frac{S_{\mathrm{TO},j}\,\omega_{\mathrm{TO},j}^2}{\omega_{\mathrm{TO},j}^2 - \omega^2 - \mathrm{i}\gamma_{\mathrm{TO},j}\,\omega}\,, \tag{8}$$

where $\omega_{\mathrm{TO},j}$, $S_{\mathrm{TO},j}$, and $\gamma_{\mathrm{TO},j}$ are the respective frequency, oscillator strength, and decay constant of the jth transverse mode, and ε_∞ is the high-frequency permittivity caused by interband electron transitions. In the quasiharmonic approximation, when $\gamma_{\mathrm{TO},j} \ll \omega_{\mathrm{TO},j}$, the expression

$$\varepsilon^{-1}(\omega) = \varepsilon_\infty^{-1} - \sum_{j=1}^{n} \frac{S_{\mathrm{LO},j}\,\omega_{\mathrm{LO},j}^2}{\omega_{\mathrm{LO},j}^2 - \omega^2 - \mathrm{i}\gamma_{\mathrm{LO},j}\,\omega} \tag{9}$$

can be obtained [11], where $\omega_{\mathrm{LO},j}$, $S_{\mathrm{LO},j}$, and $\gamma_{\mathrm{LO},j}$ are the respective frequencies, oscillator strengths, and decay constants of longitudinal optical vibrations (phonons).

Spectral dependences $\mathrm{Im}\,\varepsilon(\omega)$ and $\mathrm{Im}\,(-\varepsilon^{-1}(\omega))$ with $\varepsilon(\omega)$ in form (8) and (9) contain j maxima each at the respective frequencies $\omega_{\mathrm{TO},j}$ and $\omega_{\mathrm{LO},j}$. The width of each such peak is equal to the corresponding decay constant $\gamma_{\mathrm{TO},j}$ or $\gamma_{\mathrm{LO},j}$. The oscillator strengths of weakly decaying (when $\gamma_{\mathrm{TO},j}$, $\gamma_{\mathrm{LO},j} \ll \omega_{\mathrm{TO},j}$) transverse and longitudinal vibrational modes are described by the expressions [2, 3, 9–15]

$$S_{\mathrm{TO},j} = \frac{\gamma_{\mathrm{TO},j}}{\omega_{\mathrm{TO},j}}\,\mathrm{Im}\,\varepsilon(\omega_{\mathrm{TO},j})\,, \tag{10}$$

$$S_{\mathrm{LO},j} = \frac{\gamma_{\mathrm{LO},j}}{\omega_{\mathrm{LO},j}}\,\mathrm{Im}\,\big(-\varepsilon^{-1}(\omega_{\mathrm{LO},j})\big)\,. \tag{11}$$

The crystal permittivity $\varepsilon(\omega)$ can be calculated from the experimental reflection spectrum $R(\omega)$ using Kramers–Kronig integral relations. The parameters ε_∞, $\omega_{\mathrm{TO},j}$, $S_{\mathrm{TO},j}$, and $\gamma_{\mathrm{TO},j}$ in (8) can also be determined from the measured reflection spectrum of a sample by finding the best fit of the calculated spectrum $R(\omega)$ to the measured reflection spectrum [16].

Figure 1 shows IR reflection spectra for three $Zn_xCd_{1-x}Te$ single crystals at room temperature for normally incident nonpolarized radiation and $x = 0$ (spectrum *1*), $x = 0.05$ (spectrum *2*), and $x = 0.1$ (spectrum *3*) [12–15].

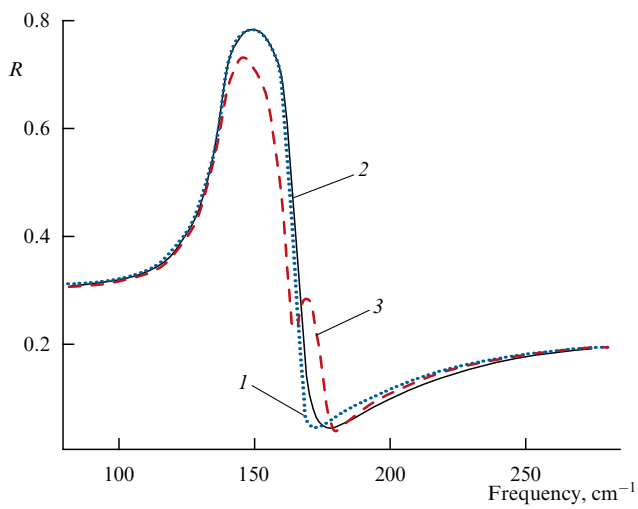

Figure 1. IR reflection spectra of CdTe (curve *1*), $Zn_{0.05}Cd_{0.95}Te$ (curve *2*), and $Zn_{0.1}Cd_{0.9}Te$ (curve *3*) single crystals [14].

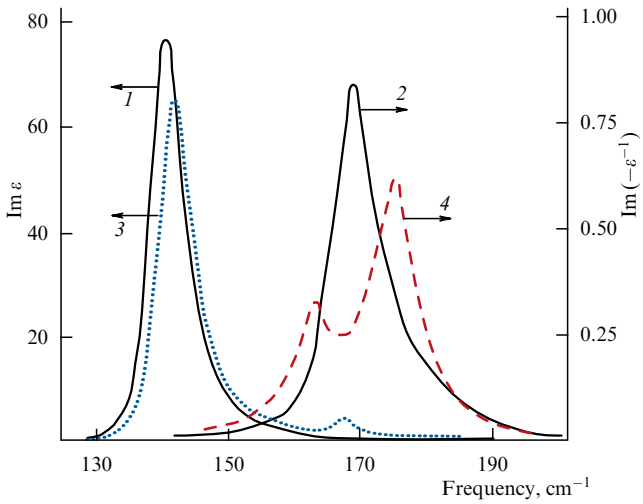

Figure 2. Functions $\mathrm{Im}\,\varepsilon(\omega)$ and $\mathrm{Im}\left(-\varepsilon^{-1}(\omega)\right)$ for $Zn_{0.05}Cd_{0.95}Te$ (curves *1* and *2*) and $Zn_{0.1}Cd_{0.9}Te$ (curves *3* and *4*) single crystals [14].

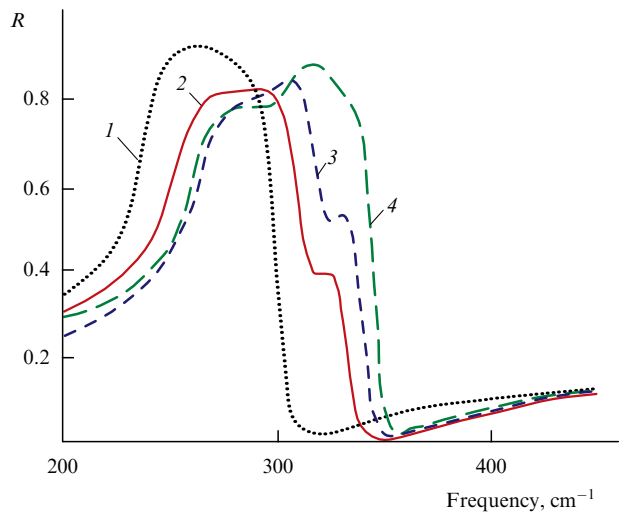

Figure 3. IR reflection spectra of single crystals of solid solutions: CdS (curve *1*), $Cd_{0.6}Zn_{0.4}S$ (curve *2*), $Cd_{0.35}Zn_{0.65}S$ (curve *3*), and $Cd_{0.2}Zn_{0.8}S$ (curve *4*) [17].

Figure 2 shows the functions $\mathrm{Im}\,\varepsilon(\omega)$ and $\mathrm{Im}\,(-\varepsilon^{-1}(\omega))$ for two single crystals $Zn_{0.05}Cd_{0.95}Te$ (curves *1* and *2*) and $Zn_{0.1}Cd_{0.9}Te$ (curves *3* and *4*), reconstructed from spectra presented in Fig. 2. The maximum of curve *1* corresponds to the optical phonon $\omega_{\mathrm{TO},1} = 139\ \mathrm{cm}^{-1}$, the first maximum of curve *3* corresponds to the phonon $\omega_{\mathrm{TO},1} = 141\ \mathrm{cm}^{-1}$, and the second, weak maximum corresponds to the phonon $\omega_{\mathrm{TO},2} = 167\ \mathrm{cm}^{-1}$. The maximum of curve *2* corresponds to the optical phonon $\omega_{\mathrm{LO},1} = 170\ \mathrm{cm}^{-1}$, while the maxima of curve *4* correspond to two longitudinal phonons at $\omega_{\mathrm{LO},1} = 176\ \mathrm{cm}^{-1}$ and $\omega_{\mathrm{LO},2} = 162\ \mathrm{cm}^{-1}$. We can clearly see from the figure that $\omega_{\mathrm{LO},2} < \omega_{\mathrm{TO},2}$.

It follows from the Lyddane–Sachs–Teller relation $\omega_{\mathrm{LO}}^2/\omega_{\mathrm{TO}}^2 = \varepsilon_0/\varepsilon_\infty$, which is valid in the strictly harmonic approximation ($\gamma = 0$) for single-oscillator crystals [2], that $\omega_{\mathrm{LO}}-\omega_{\mathrm{TO}} \approx (\varepsilon_0-\varepsilon_\infty)\omega_{\mathrm{TO}}/2\varepsilon_\infty$. For $\omega_{\mathrm{LO},2} < \omega_{\mathrm{TO},2}$, the quantity $\omega_{\mathrm{LO},2} - \omega_{\mathrm{TO},2} \approx (\varepsilon_0^{\mathrm{loc}} - \varepsilon_\infty^{\mathrm{loc}})\omega_{\mathrm{TO},2}/2\varepsilon_\infty^{\mathrm{loc}}$ is negative, which means that the oscillator strength of this phonon, $S_{\mathrm{TO},2} = (\varepsilon_0^{\mathrm{loc}} - \varepsilon_\infty^{\mathrm{loc}}) = (\gamma_{\mathrm{TO},2}/\omega_{\mathrm{TO},2})\mathrm{Im}\,\varepsilon(\omega_{\mathrm{TO},2})$, is also negative. Here, $\varepsilon_\infty^{\mathrm{loc}}$ and $\varepsilon_0^{\mathrm{loc}}$ are the effective permittivities at respective frequencies $\omega > \omega_{\mathrm{TO},2}$ and $\omega < \omega_{\mathrm{LO},2}$ [9, 10]. We note that both these additional phonons, $\omega_{\mathrm{TO},2}$ and $\omega_{\mathrm{LO},2}$, are located in the frequency range between $\omega_{\mathrm{TO},1}$ and $\omega_{\mathrm{LO},1}$. It is in this frequency region that the real part of the permittivity of crystals is negative [12–15].

Figure 3 presents the reflection spectra of $Cd_{1-x}Zn_xS$ single crystals of solid solutions at room temperature for normally incident linearly polarized IR radiation with $E \perp c$ (c is the optical axis of the crystal) for $x = 0$ (curve *1*), $x = 0.40$ (curve *2*), $x = 0.65$ (curve *3*), and $x = 0.80$ (curve *4*) [17].

The functions $\mathrm{Im}\,\varepsilon(\omega)$ and $\mathrm{Im}\,(-\varepsilon^{-1}(\omega))$ were obtained from these spectra, and the frequencies of optical phonons and their oscillator strengths were calculated using these functions. Figure 4 shows the dependence of optical phonon frequencies for $Cd_{1-x}Zn_xS$ single crystals of solid solutions on the solid solution composition. Along with the fundamental band of residual rays, the spectra of solid solutions exhibit a weak band absent in the spectra of pure components (ZnS and CdS).

The vibrational frequencies of impurity atoms (in the mass defect approximation) are well described by the

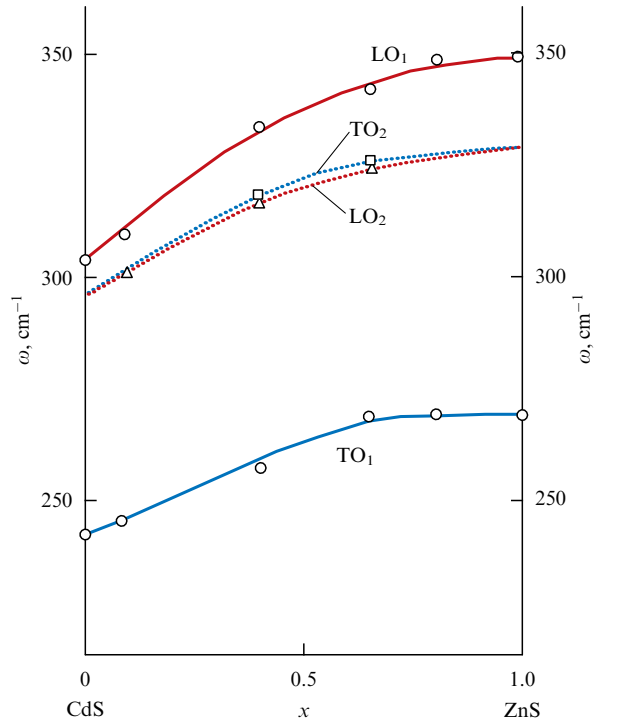

Figure 4. Dependences of optical phonon frequencies in $Cd_{1-x}Zn_xS$ single crystals on the solid solution composition [17, 19].

Vinogradov theory [18] at concentrations $x < 0.3$ and $1 - x < 0.3$ if the density of optical phonons and vibration amplitudes of atoms in crystals without impurities are known. It was shown in [19] that theoretical calculations of the $Zn_{1-x}Cd_xS$ solid solutions [18] using the phonon density in ZnS from [20] described the experimental results in [17] unexpectedly well in the whole concentration range, including the frequencies of additional (inverted) phonons, without fitting parameters. Additional phonons in $Zn_{1-x}Cd_xS$ were assigned to quasilocal vibrations of Cd and ZnS atoms. These quasilocal vibrations fall into the quasigap in the optical phonon density in ZnS [9, 10, 19].

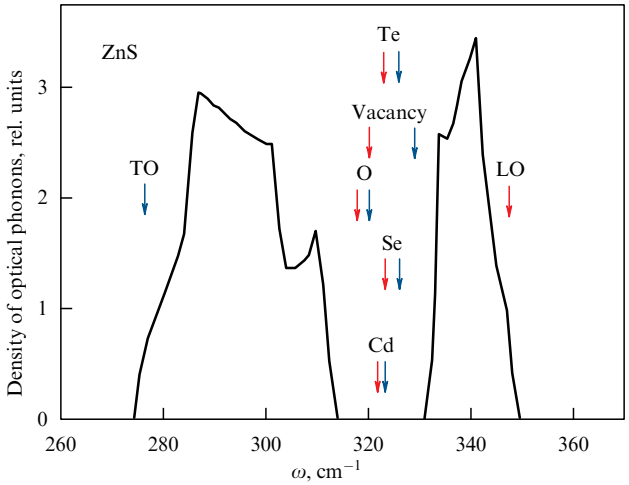

Figure 5. (Color online.) Density of optical phonons in a cubic ZnS crystal [16]. The frequencies of optical phonons are $\omega_{TO} = 276$ cm^{-1} and $\omega_{LO} = 350$ cm^{-1}. The arrows show the vibrational frequencies of impurity atoms replacing sulfur atoms and also the vibrational frequencies of sulfur atom vacancies falling into the quasigap in the density of optical phonons: blue and red arrows are the respective transverse and longitudinal vibrations of impurity atoms. The calculation is performed for the concentration of impurity atoms 20% [9, 10, 21].

Figure 5 shows the results of the solution of the Vinogradov equation for several impurity atoms substituting sulfur atoms in ZnS with $m^* = 0$ (sulfur atom vacancy), $m^* = 16$ (oxygen), $m^* = 79$ (selenium), $m^* = 127.6$ (tellurium), and $m^* = 112.4$ (cadmium substituting Zn atoms).

The dispersion of optical phonons in the Brillouin zone is small for almost all the A^2B^6 compounds and is comparable to the LO–TO splitting in a crystal field at the center of the Brillouin zone. As a result, the density of optical phonons splits, as it were, into the density of transverse optical phonons and the density of longitudinal phonons, and a quasigap with a small density of states appears between them. The quasilocal (or quasiresonance) vibrations of many impurity atoms substituting S and (or) Zn in ZnS fall just into this quasigap. As mentioned, the real part of the permittivity is negative in the frequency range between the TO and LO phonons of pure ZnS, which causes the frequency inversion of longitudinal and transverse vibrations of impurity atoms, thereby making the oscillator strength of these vibrations negative.

The reflection spectra of the family of $ZnSe_xS_{1-x}$ crystals also exhibit additional inverted optical phonons in the high-frequency band of residual rays (in ZnS-like modes) in the form of a small dip [21–23]. The frequency range between the ZnS-like TO and LO modes contains two additional modes. One of them (at ~ 300 cm^{-1}), clearly observed in Raman spectra and enhanced due to the Fermi resonance, is assigned to a second-order line, while the other (near 320 cm^{-1}) is assigned to the quasiresonance mode of impurity Se atoms for small x [21–23]. Figure 6 presents the frequencies of optical phonons obtained from IR reflection spectra [21–23]. The concentration dependence of the ZnS- and ZnSe-like TO and LO modes is unambiguously interpreted as the two-mode behavior of optical phonons in solid solutions and agrees well with the results of all the known studies of optical phonons in $ZnSe_xS_{1-x}$.

The additional 320 cm^{-1} mode has an inverted TO–LO doublet, which is well confirmed by calculations for vibrations of the Se impurity in a ZnS crystal in the microscopic theory of the crystal lattice dynamics at low impurity concentrations [9, 21] (see Fig. 5). The additional ~ 300 cm^{-1} mode also demonstrates the inverted TO–LO doublet. This mode is also observed in Raman spectra and is assigned to a second-order line [21–23].

It was previously assumed in [7, 8] that in solid $A_{1-x}B_xC$ solutions, in addition to usual normal dipole oscillators $A-C$ and $B-C$, the $A-B$ oscillator can also be active. It follows from (3) that the effective microscopic ion charge e_S^* can be determined from experimental data. This charge was previously measured for A^2B^6 compounds with an accuracy of ± 0.02 [24] to be $e_S^*(\text{ZnS}) = 0.88e$; $e_S^*(\text{ZnSe}) = 0.72e$; $e_S^*(\text{ZnTe}) = 0.65e$; $e_S^*(\text{CdS}) = 0.87e$; $e_S^*(\text{CsSe}) = 0.83e$; and

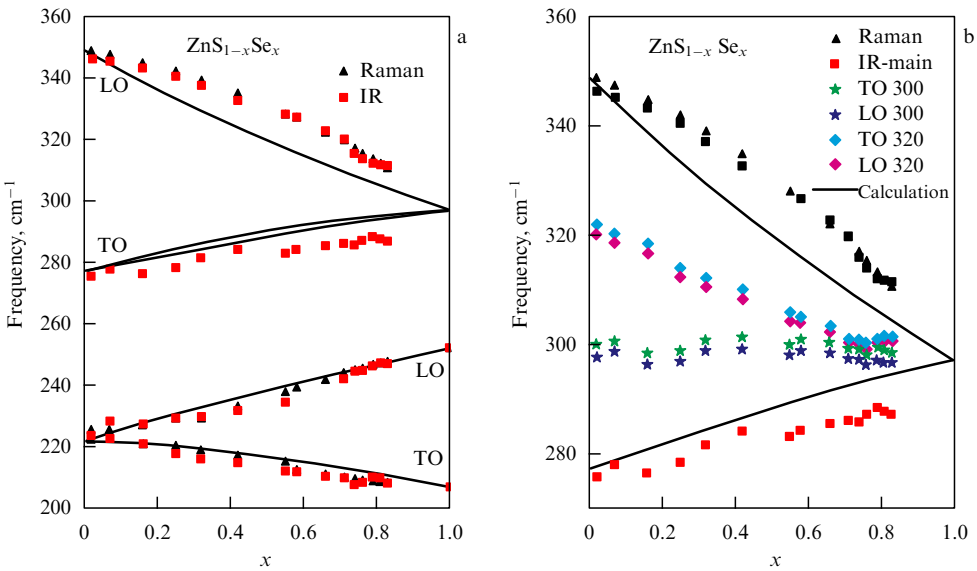

Figure 6. Concentration dependences of optical phonon frequencies in $ZnSe_xS_{1-x}$ single crystals obtained from IR reflection spectra and Raman spectra [21–23]. (a) Main optical phonons. (b) Additional optical phonons inside the LO–TO-splitting on the main ZnS-like phonons; located between them are the two branches of inverted phonons converging to the local vibration frequency of sulfur atoms in ZnSe.

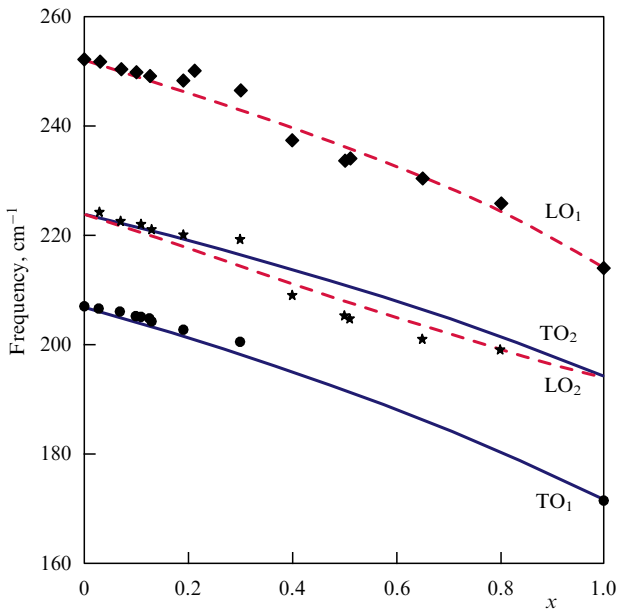

Figure 7. Concentration dependences of optical vibration frequencies of atoms in a $Zn_{1-x}Cd_xSe$ solid solution: solid and dashed curves are calculated for transverse and longitudinal modes, respectively. Symbols are experimental data [25, 26].

$e_S^*(\mathrm{CdTe}) = 0.74e$. Thus, for the $ZnSe_xS_{1-x}$ alloy, the difference between the charges of sulfur and selenium ions under the replacement of sulfur atoms by selenium atoms is $0.16e$. This means that in an electrically neutral crystal cell of a solid solution, an S–Se dipole should appear with an oscillator strength one tenth that of the Zn–S and Zn–Se dipoles, because its charge is $\pm 0.08e$, and not about $0.8e$, as for pure compounds. We can see from experimental values of ion charges in the A^2B^6 compounds presented above that an S–Se dipole can exist in a solid $ZnSe_xS_{1-x}$ solution.

In the system of solid $Zn_{1-x}Cd_xSe$ solutions, additional inverted phonons were also discovered in the frequency range where the real part of the crystal permittivity is negative: between fundamental TO and LO phonons [25, 26]. The reflection spectra of single crystals of solid $Zn_{1-x}Cd_xSe$ solutions look similar to the spectra of $Zn_{1-x}Cd_xS$ crystals (Fig. 3). These spectra were used to obtain the frequency dependence of the crystal permittivity, optical phonon frequencies, phonon lifetimes, and oscillator strengths. Figure 7 presents the concentration dependences of optical phonon frequencies in $Zn_{1-x}Cd_xSe$ crystals.

The authors of [25] theoretically found the normal vibrations of atoms in the isodisplacement model [6] taking the interaction of ZnSe- and CdSe-like vibrations into account. The fundamental assumption of this model is that the anions and cations of ZnSe (CdSe) groups vibrate in phase with the same amplitude, and each ion is subjected to forces statistically averaged over all neighbors. The concentration dependences of optical mode frequencies (Fig. 7) and oscillator strengths (Fig. 8) calculated for solid $Zn_{1-x}Cd_xSe$ solutions agree well with experimental data.

The atomic displacement amplitudes have also been calculated (Fig. 9). It is shown that except for the Zn–Se and Cd–Se dipoles, vibrations exist in which Se atoms are in fact immobile, while the Zn and Cd atoms vibrate with respect to each other, forming a weak Zn–Cd dipole.

For $x = 0$, the Zn and Se atoms oscillate out of phase in the fundamental mode, which is well known for the optical mode in a ZnSe crystal. As x increases, the Cd atoms start taking part in these oscillations. They oscillate in phase with Zn atoms and their amplitude increases, whereas the oscillation amplitude of Zn atoms decreases. We note that the oscillation amplitude of Se atoms very weakly depends on the solid solution composition.

In the quasiresonance mode with inverted LO–TO phonon frequencies, the Cd and Zn atoms oscillate out of phase, while the participation of Se atoms in this mode is insignificant [25]. As x increases, the displacement amplitude of Cd atoms decreases, but the displacement amplitude of Zn atoms oscillating out of phase with Cd atoms increases. The dipole moment appearing during these oscillations is determined by the difference between the effective charges of Zn and Cd ions. This difference is small and the dipole moment of the Zn–Cd oscillations is just over 10% the dipole moment of the fundamental (Zn–Se or Cd–Se) oscillations. This

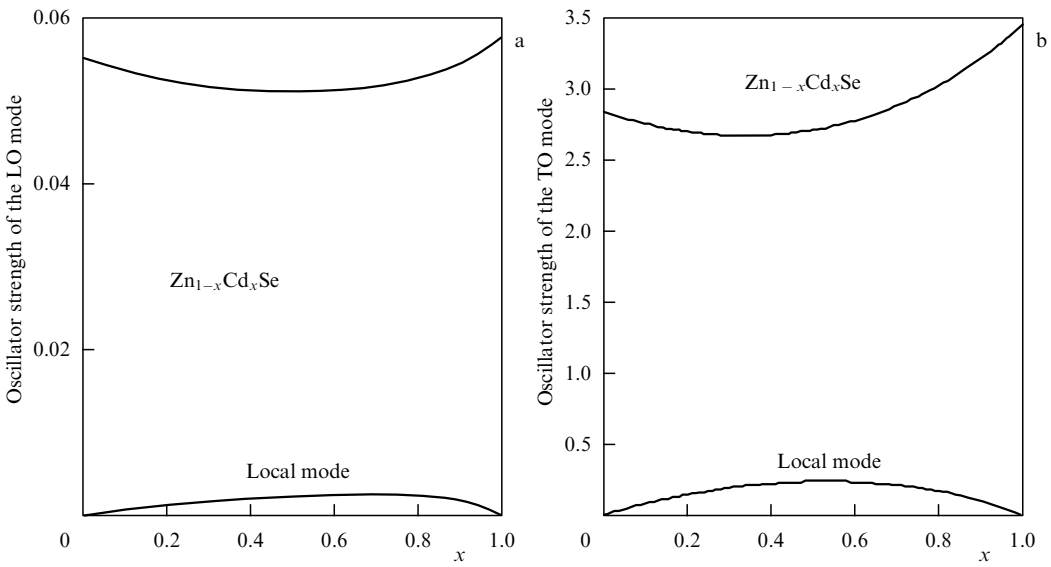

Figure 8. Concentration dependences of the oscillator strengths for (a) longitudinal and (b) transverse modes in a $Zn_{1-x}Cd_xSe$ solid solution.

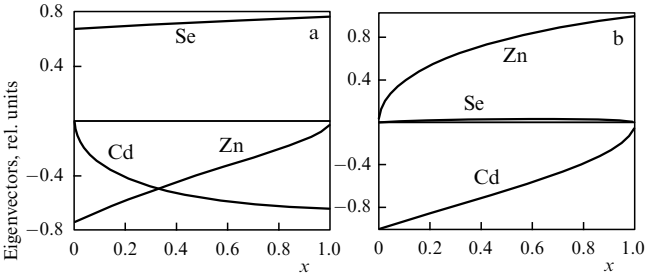

Figure 9. Concentration dependences of the displacement amplitudes of atoms in a $Zn_{1-x}Cd_xSe$ solid solution for normal vibrations in (a) the fundamental mode and (b) the local mode [25].

corresponds to a small oscillator strength for Zn–Cd oscillations and a low intensity of the Raman peaks and the functions $\mathrm{Im}\,\varepsilon(\omega)$ and $\mathrm{Im}(-\varepsilon^{-1}(\omega))$ in the Zn–Cd mode [15, 25, 26].

3. Conclusions

An analysis of data on the dispersion and the density of states of optical phonons [20] in ion–covalent crystals has shown that the density of states of optical phonons in almost all crystals of A^1B^7 and A^2B^6 compounds and some A^3B^5 crystals has a dip at frequencies between the LO and TO phonons in the center of the Brillouin zone. This dip (quasigap) in ZnS most clearly divides the density of optical phonons into two parts, with transverse optical phonons dominating in the low-frequency part and longitudinal phonons in the high-frequency part. The local vibrations of impurity atoms fall just into the quasigap. The real part of the crystal permittivity in the quasigap is negative; the longitudinal–transverse splitting of vibrations of impurity atoms proves to be inverted, i.e., the longitudinal vibrations of impurity atoms have lower frequencies than do transverse vibrations.

It follows from (3) that the LO–TO splitting at the Brillouin zone center is proportional to the dynamical ion charge e_S^* squared. Because of the different ionicity of binary solutions (different charges e_S^*), additional weak dipoles appear, as predicted in [7, 8]. In our case, these are local dipole oscillations of Zn–Cd ions in solid $Zn_{1-x}Cd_xS$, $Zn_{1-x}Cd_xSe$, and $Zn_{1-x}Cd_xTe$ solutions and weak S–Se and $ZnSe_xS_{1-x}$ dipoles. The oscillator strength of these local vibrations is negative: they seem to borrow the oscillator strength from fundamental phonons of crystals. Their discovery resolves the contradiction related to the apparent violation of selection rules. Two-phonon states can also fall into the quasigap, as was observed in $ZnSe_xS_{1-x}$ crystals at frequencies close to 300 cm^{-1} [23]. Inverted optical phonons were discovered earlier in the low-temperature phase in the α-β structural phase transition in crystalline quartz ($T_c = 846$ K) [27, 28]. In the temperature range from 800 K to 300 K, a narrow dip is observed in the high-frequency band of residual rays (E-phonons) in IR reflection spectra. This dip is related to the appearance of additional frequency-inverted optical phonons caused by the interaction of the E-phonons with the A_2-phonons forbidden in the given geometry [27, 28].

Inverted oscillators with a negative oscillator strength can appear not only in purely phonon spectra of impurity crystals. For example, the authors of [29–31] discovered the effect of interaction of the 4f-electron excitations corresponding to the transition to the first excited Stark level of the Pr^{+3} ion in a $PrFe_3(BO_3)_4$ crystal when it falls into the LO–TO splitting region of a low-frequency phonon of a crystal of the same symmetry. In this case, the corresponding electron–phonon oscillator is inverted, and its longitudinal frequency becomes smaller than the transverse frequency.

We note that the oscillator strengths of optical phonons and effective ion charges obtained from experimental spectra along with standard phonon-frequency and lifetime measurements allow one to better understand and explain the features of IR and Raman spectra of crystals observed in experiments. We also note that IR reflection spectra are always obtained from the crystal surface, and the surface layer typically contains many packing defects, such as vacancies, variable interatomic distances, and defects produced by the mechanical polishing of crystals. Figure 3 shows that vibrations of vacancies can also fall into the quasigap in the density of optical phonons, producing the feature in the reflection spectrum discussed here.

Acknowledgments
This paper was stimulated by a discussion of the nature of inverted oscillators with M N Popova and K N Boldyrev.

References

1. Kellermann E W *Philos. Tans. R. Soc. Lond. A* **238** 513 (1940)
2. Born M, Kun Huang *Dynamical Theory of Crystal Lattices* (Oxford: Clarendon Press, 1954); Translated into Russian: *Dinamicheskaya Teoriya Kristallicheskikh Reshetok* (Moscow: IL, 1958)
3. Balkanski M, in *Proc. of the Intern. Conf. on II – VI Semiconducting Compounds, Rhode Islands, Flammarion, 1963* (Rhode Islands: Flammarion, 1963) p. 1007
4. Szigeti B *Trans. Faraday Soc.* **45** 155 (1949)
5. Hayes W, Loudon R *Scattering of Light by Crystals* (New York: Wiley, 1978)
6. Genzel L, Martin T P, Perry C H *Phys. Status Solidi B* **62** 83 (1974)
7. Jahne E *Phys. Status Solidi B* **74** 275 (1976)
8. Jahne E *Phys. Status Solidi B* **75** 221 (1976)
9. Vinogradov E A et al. *Phys. Usp.* **52** 290 (2009); *Usp. Fiz. Nauk* **179** 313 (2009)
10. Vinogradov E et al. *Phys. Status Solidi B* **247** 1480 (2010)
11. Belousov M V *Sov. Phys. Solid State* **15** 813 (1973); *Fiz. Tverd. Tela* **15** 1206 (1973)
12. Vodop'yanov L K, Vinogradov E A, Vinogradov V S *Sov. Phys. Solid State* **16** 545 (1974); *Fiz. Tverd. Tela* **16** 849 (1974)
13. Vodopyanov L K, Vinogradov E A *Cryst. Lattice Defects* **5** 125 (1974)
14. Mavrin B N, Vinogradov E A, in *CdTe and Related Compounds; Physics, Defects, Technology, Hetero- and Nano-structures Crystal Growth, Surfaces and Applications* Pt. 1 (Eds R Triboulet, P Siffert) (Amsterdam: Elsevier, 2009) p. 22
15. Vinogradov E A, Vodop'yanov L K *Sov. Phys. Solid State* **17** 2088 (1975); *Fiz. Tverd. Tela* **17** 3161 (1975)
16. Theiss W "SCOUT. Hard- and Software for Optical Spectroscopy", Technical Manual (2019)
17. Mityagin Yu A, Vodop'yanov L K, Vinogradov E A *Sov. Phys. Solid State* **17** 1341 (1975); *Fiz. Tverd. Tela* **17** 2054 (1975)
18. Vinogradov V S *Sov. Phys. Solid State* **11** 1666 (1969); *Fiz. Tverd. Tela* **11** 2062 (1969)
19. Vinogradov E A, Mityagin Yu A *Sov. Phys. Solid State* **20** 1825 (1978); *Fiz. Tverd. Tela* **20** 3162 (1978)
20. Bilz H, Kress W *Phonon Dispersion Relations in Insulators* (Springer Series in Solid-State Sciences, Vol. 10) (Berlin: Springer-Verlag, 1979)
21. Vinogradov E A et al., in *Modern Problems of Laser Physics, MPLP'2008, Proc. of the 5th Intern. Symp., August 24 – 30, Novosibirsk, Russia* (Eds S N Bagayev, P V Pokassov) (Novosibirsk: Inst. of Laser Physics SB RAS, 2009) p. 3
22. Vinogradov E A et al. *Phys. Solid State* **48** 1940 (2006); *Fiz. Tverd. Tela* **48** 1826 (2006)

23. Vinogradov E A et al. *Laser Phys*. **19** 162 (2009)
24. Vinogradov E A *Extended Abstract of Cand. Sci.* (Phys.-Math) Dissertation (Dolgoprudnyi, MIPT, 1973)
25. Vinogradov E A, Mavrin B N, Vodop'yanov L K *J. Exp. Theor. Phys*. **99** 749 (2004); *Zh. Eksp. Teor. Fiz*. **126** 866 (2004)
26. Vodopyanov L K et al. *Phys. Status Solidi C* **1** 3162 (2004)
27. Scott J F, Porto S P S *Phys. Rev*. **161** 903 (1967)
28. Gervais F, Piriou B *Phys. Rev. B* **11** 3944 (1975)
29. Boldyrev K N et al. *Phys. Rev. B* **90** 121101(R) (2014)
30. Boldyrev K N et al. *Phys. Rev. Lett*. **118** 167203 (2017)
31. Popova M N, Boldyrev K N *Phys. Usp*. **62** 275 (2019); *Usp. Fiz. Nauk* **189** 292 (2019)